

Crystal Structures of DPP-IV (CD26) from Rat Kidney Exhibit Flexible Accommodation of Peptidase-Selective Inhibitors

Kenton L. Longenecker,^{*,‡} Kent D. Stewart,[‡] David J. Madar,[§] Clarissa G. Jakob,[‡] Elizabeth H. Fry,[‡] Sherwin Wilk,^{||} Chun W. Lin,[§] Stephen J. Ballaron,[§] Michael A. Stashko,[§] Thomas H. Lubben,[§] Hong Yong,[§] Daisy Pireh,[§] Zhonghua Pei,[§] Fatima Basha,[§] Paul E. Wiedeman,[§] Thomas W. von Geldern,[§] James M. Trevillyan,[§] and Vincent S. Stoll[‡]

Department of Structural Biology and Department of Metabolic Disease, Global Pharmaceutical Research and Development, Abbott Laboratories, Abbott Park, Illinois 60064-6098, and Department of Pharmacology, Mount Sinai School of Medicine, New York, New York 10029

Received January 27, 2006; Revised Manuscript Received April 28, 2006

ABSTRACT: Dipeptidyl peptidase IV (DPP-IV) belongs to a family of serine peptidases, and due to its indirect regulatory role in plasma glucose modulation, DPP-IV has become an attractive pharmaceutical target for diabetes therapy. DPP-IV inactivates the glucagon-like peptide (GLP-1) and several other naturally produced bioactive peptides that contain preferentially a proline or alanine residue in the second amino acid sequence position by cleaving the N-terminal dipeptide. To elucidate the details of the active site for structure-based drug design, we crystallized a natural source preparation of DPP-IV isolated from rat kidney and determined its three-dimensional structure using X-ray diffraction techniques. With a high degree of similarity to structures of human DPP-IV, the active site architecture provides important details for the design of inhibitory compounds, and structures of inhibitor–protein complexes offer detailed insight into three-dimensional structure–activity relationships that include a conformational change of Tyr548. Such accommodation is exemplified by the response to chemical substitution on 2-cyanopyrrolidine inhibitors at the 5 position, which conveys inhibitory selectivity for DPP-IV over closely related homologues. A similar conformational change is also observed in the complex with an unrelated synthetic inhibitor containing a xanthine core that is also selective for DPP-IV. These results suggest the conformational flexibility of Tyr548 is unique among protein family members and may be utilized in drug design to achieve peptidase selectivity.

Inhibition of the proteolytic enzyme dipeptidyl peptidase IV (DPP-IV,¹ EC 3.4.15.5) is increasingly appreciated as a potential therapeutic strategy for non-insulin-dependent (type 2) diabetes, a major world health concern (1, 2). DPP-IV is believed to be responsible for the rapid inactivation of glucagon-like peptide 1 (GLP-1), which is a naturally produced bioactive peptide that enhances insulin secretion and inhibits glucagon release upon oral ingestion of nutrients (3). The bioactivity of GLP-1 influences multiple aspects of glucose homeostasis and importantly promotes normalization of blood glucose levels in diabetic patients. The therapeutic rationale for DPP-IV inhibition is to extend the half-life of GLP-1 bioactivity and thereby improve the impaired glucose tolerance of the diabetic patient. DPP-IV may also mediate additional effects by processing other bioactive peptides such

as gastric inhibitory peptide, substance P, bradykinin, neuropeptide Y, and various chemokines and cytokines, so the consequences of DPP-IV inhibition are of special interest in ongoing in vivo investigations (4).

In addition to possessing peptidase activity, DPP-IV may impact functions of the immune system, potentially acting as a costimulatory protein on the surface of T-cells through interactions with other proteins (5). For some time, the physiological binding partner of adenosine deaminase (ADA) was ascribed to a protein of unknown sequence named CD26, but its identity with DPP-IV is now recognized. However, the functional consequences of ADA binding are uncertain and continue to be an area of ongoing research. In contrast to many mammalian species, rat DPP-IV lacks ADA binding activity and provides an important comparison to its relatives. Recent structural results on complexes of DPP-IV and ADA have defined the interacting surfaces and suggest structural differences for the functional variation among species (6, 7).

Many physical characteristics underlying the function of DPP-IV (CD26) are known (8). DPP-IV is found in two forms in the body, consisting of a membrane-bound form that is tethered to extracellular surfaces and a soluble form that circulates in the plasma. The immobilized form is tethered by an N-terminal peptide sequence of ~35 residues that upon cleavage yields the soluble form. DPP-IV belongs

* To whom correspondence should be addressed: Department of Structural Biology, R46Y, Bldg. AP10, 100 Abbott Park Rd., Abbott Park, IL 60064. Phone: (847) 938-1428. Fax: (847) 937-2625. E-mail: Kenton.Longenecker@Abbott.com.

[‡] Department of Structural Biology, Global Pharmaceutical Research and Development, Abbott Laboratories.

[§] Department of Metabolic Disease, Global Pharmaceutical Research and Development, Abbott Laboratories.

^{||} Mount Sinai School of Medicine.

¹ Abbreviations: GLP-1, glucagon-like peptide 1; DPP-IV, dipeptidyl peptidase IV; ADA, adenosine deaminase; POP, prolyl oligopeptidase; rmsd, root-mean-square deviation.

to a class of serine-type peptidases, with the residues of the catalytic triad occurring in the nonclassical Ser-Asp-His amino acid sequence order, characteristic of its structural subfamily that includes DPP-8, DPP-9, and FAP (fibroblast activation protein) as its closest relatives (9). DPP-IV cleaves dipeptides from the N-terminus of substrates that preferentially contain a proline or alanine in the P1 position (10) but shows no significant specificity for particular residue types at other positions. While DPP-IV peptidase activity is inhibited by a variety of small molecule synthetic compounds, a class of acylated cyanopyrrolidines was discovered to be a particularly potent core and provided an important foundation for medicinal chemistry efforts (11). Representatives of the cyanopyrrolidine series have progressed to clinical evaluation, and analogues are of great pharmaceutical interest (12).

In an effort to elucidate the details of the active site, we crystallized a natural source preparation of DPP-IV purified from rat kidney and determined its three-dimensional structure. With a high degree of similarity to human DPP-IV, the structure exhibits an α/β -hydrolase protein fold and an additional domain that forms an eight-blade β -propeller, which effectively limits access to the active site and contributes to the observed substrate specificity. Because the protein was isolated directly from rat tissue, we gain insight into the natural post-translational glycosylation and note structural differences with relatives from different species that bind adenosine deaminase (ADA). The results also offer detailed information for structure-based drug design and provide an accessible means of experimentally determining binding modes of inhibitory compounds. On the basis of studies of complexes with synthetic inhibitors, we highlight the conformational flexibility of the protein to accommodate certain compounds that selectively inhibit DPP-IV over related dipeptidyl peptidases.

EXPERIMENTAL PROCEDURES

Protein Purification. DPP-IV was purified to electrophoretic homogeneity from rat kidney essentially as described previously (11). The enzyme was solubilized by autolysis for 18 h at 37 °C, precipitated by saturation to 90% with $(\text{NH}_4)_2\text{SO}_4$, and subjected to sequential chromatography on Superose S-300, DEAE Sephacel, and phenyl-Sepharose. The purified enzyme was dialyzed against 0.05 M Tris-HCl (pH 7.5) and concentrated by ultrafiltration to 6–7 mg/mL. The specific activity of the preparation was 15.3 units/mg, where 1 unit catalyzes the release of 1 mmol of 2-naphthylamine from Ala-Pro-2-naphthylamide per minute at 37 °C.

Crystallization and Structure Determination. Purified protein was crystallized by vapor diffusion with a reservoir solution of 2.8 M ammonium sulfate and 100 mM sodium acetate (pH 4.2), placing 1 μL of protein mixed with 1 μL of reservoir solution over a 1 mL reservoir in a 24-well plate at 17 °C. Heavy atom derivatives and complexes with inhibitory compounds were prepared by soaking crystals with compound in stabilization solution [3 M ammonium sulfate and 100 mM sodium acetate (pH 5.0)] and briefly transferring the samples into cryoprotectant buffer [3 M ammonium sulfate, 100 mM sodium acetate (pH 5.0), and 25% xylitol] for preservation in liquid nitrogen. X-ray data were collected at the Advanced Photon Source of Argonne National

Laboratory on IMCA beamline 17-ID at a 1 Å wavelength using an ADSC quantum 210 detector. Data were integrated and scaled using HKL2000 (13), and intensities were converted to structure factor magnitudes using TRUNCATE within the CCP4 program suite (14, 15). The diffraction data exhibited cubic symmetry of the $P2_13$ space group with unit cell dimensions of 208 Å. Four heavy atom derivatives were used to determine the structure by multiple isomorphous replacement with anomalous scattering (MIRAS). Initial calculations using SOLVE (16) correctly identified nine Pt sites in a PtCl_4 derivative and 10 Pt sites in a diplatinum-iodoethylenediamine (PIP) derivative, yielding a Z-score of 42 and a figure of merit of 0.52 for data to 4 Å. Refinement and inclusion of data from derivatives prepared with AuCl_4 and thimerosal allowed experimental phasing to 3.3 Å resolution. Subsequent density modification using DM yielded an interpretable electron density map. A protein model was built and refined using O (17) and QUANTA and CNX (Accelrys), targeting the measured structure factor magnitudes and HL coefficients containing the experimentally determined phase information. Figures were prepared using InsightII (Accelrys) and PyMOL (DeLano Scientific). Atomic coordinates of the structures were deposited in the Protein Data Bank as the following entries: 2GBC (apo), 2GBF (inhibitor 1), 2GBG (inhibitor 2), and 2GBI (inhibitor 4).

Activity Measurement of Inhibitory Compounds. Kinetic analysis was performed on the purified rat DPP-IV protein and recombinant preparations of human DPP-IV, DPP-8, and DPP-9 in assays that determined equilibrium rates of cleavage of Gly-Pro-7-amidomethylcoumarin with a matrix of conditions of both substrate and inhibitors, and details will be published elsewhere. Briefly, apparent (inhibited) and noninhibited K_m and V_{\max} values, determined from the nonlinear fitting of Michaelis–Menten plots, were used to determine kinetic constants for competitive (K_{ic}) inhibition. They were also used to determine that uncompetitive inhibition of DPPIV by these compounds did not occur. Inhibitory compounds were prepared by the methods described in published literature (18, 19).

RESULTS AND DISCUSSION

Overall Structure of Rat DPP-IV. Rat kidney DPP-IV was solubilized by autolysis and isolated as previously described with an observed molecular mass of 110 kDa, which differs from the predicted value of 84 kDa for the amino acid sequence due to post-translational glycosylation (11). In contrast to reports of DPP-IV crystallization from other preparations at basic pH with polyethylene glycols, the rat protein crystallized with ammonium sulfate at acidic pH and diffracted X-rays to 2.8 Å resolution. The closest relative with a known structure at the time of structure determination was prolyl oligopeptidase (20), which did not provide an adequate model for molecular replacement, so the structure was determined experimentally by heavy atom multiple isomorphous replacement. A model that contains the continuous peptide sequence for rat DPP-IV from residue 38 through 767 was built and refined (Table 1).

The asymmetric unit contains a dimer of protein molecules that are essentially identical, and the structure was refined using tight noncrystallographic restraints throughout. Because

Table 1: X-ray Data and Model Refinement Statistics

| X-ray Diffraction Data | | | | |
|---|---|------------------------|------------------------|--------------------------|
| | apo | inhibitor 1 | inhibitor 2 | inhibitor 4 |
| resolution limit (Å) | 2.8 | 3.1 | 3.0 | 3.3 |
| no. of observations | 387639 | 310384 | 419958 | 340435 |
| no. of unique observations | 73192 | 54268 | 59362 | 45578 |
| completeness (%) | 99 (97) ^a | 99.8 (99) ^a | 99.4 (99) ^a | 99.9 (99.8) ^a |
| <i>I</i> / <i>σ</i> _{<i>I</i>} | 13 (2.5) ^a | 8 (2.5) ^a | 8 (2.6) ^a | 5.5 (3.2) ^a |
| <i>R</i> _{sym} ^b (%) | 8.9 (47) ^a | 12.5 (53) ^a | 10.6 (69) ^a | 17 (63) ^a |
| MIRAS Phasing | | | | |
| derivatives | PtCl ₄ (3.7 Å, 9 Pt sites), PIP (3.8 Å, 16 Pt sites), AuCl ₄ (3.5 Å, 7 Au sites), thimerosal (3.2 Å, 4 Hg sites) | | | |
| figure of merit ^c (20–3.3 Å) | 0.49 (SOLVE), 0.69 (DM) | | | |
| Model Refinement | | | | |
| | apo | inhibitor 1 | inhibitor 2 | inhibitor 4 |
| no. of reflections (work/free) | 69035/3673 | 51017/2743 | 56080/2997 | 43085/2293 |
| completeness (work/free) (%) | 94/5 | 94/5 | 94/5 | 95/5 |
| <i>R</i> _{factor} ^d (work/free) (%) | 22.8/25.8 | 24.7/28.8 | 23.3/26.9 | 23.7/27.8 |
| mean <i>B</i> factor | 64 | 66 | 58 | 41 |
| rmsd for ideal bond lengths (Å) | 0.008 | 0.009 | 0.009 | 0.009 |
| rmsd for ideal bond angles (deg) | 1.47 | 1.53 | 1.52 | 1.55 |
| rmsd for NCS α-carbons (Å) | 0.028 | 0.026 | 0.025 | 0.025 |

^a Values in parentheses are for the highest-resolution shell. ^b *R*_{sym} = $\sum |I - \langle I \rangle| / \sum I$, where *I* is the integrated intensity for a reflection. ^c Figure of merit = $\langle \sum P(\alpha) e^{i\alpha} / \sum P(\alpha) \rangle$, where *P*(α) is the phase probability at angle α. ^d *R*_{factor} = $\sum |F_P - F_C| / \sum F_P$, where *F*_P and *F*_C are the observed and calculated structure factor amplitudes, respectively, while *R*_{free} is calculated on 5% of the data excluded from refinement.

^a Values in parentheses are for the highest-resolution shell. ^b $R_{\text{sym}} = \sum |I - \langle I \rangle| / \sum I$, where I is the integrated intensity for a reflection. ^c Figure of merit = $\langle \sum P(\alpha) e^{i\alpha} / \sum P(\alpha) \rangle$, where $P(\alpha)$ is the phase probability at angle α . ^d $R_{\text{factor}} = \sum |F_o - F_c| / \sum F_o$, where F_o and F_c are the observed and calculated structure factor amplitudes, respectively, while R_{free} is calculated on 5% of the data excluded from refinement.

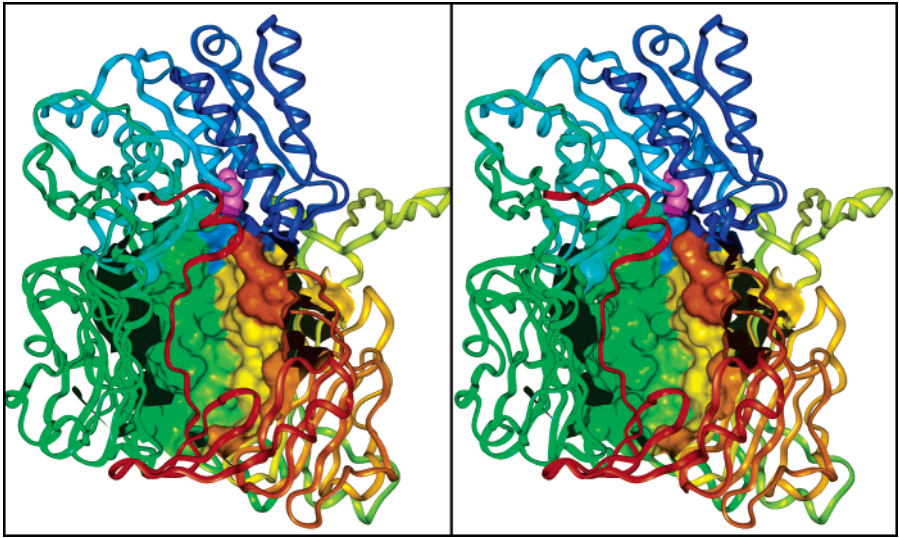


FIGURE 1: Structure of rat DPP-IV (stereoview). The ribbon diagram is colored from the N-terminus to the C-terminus as a gradation from red to blue. A portion of the enzyme's surface is rendered to highlight the interior cavity of the protein, and the catalytic serine residue is colored magenta.

the protein is observed to behave as a dimer in solution, the noncrystallographic dimer is thought to be biologically relevant, burying 2116 Å² of each monomer across the interface, while no other intermolecular lattice contacts suggest additional oligomeric structures that are significant in vivo. The monomer consists of two domains comprised of an N-terminal eight-blade β -propeller and a slightly smaller C-terminal catalytic domain (residues 509–767) that adopts an α/β -hydrolase fold (Figure 1). The active site is located inside a large solvent-filled cavity surrounded by the propeller, reminiscent of the prolyl oligopeptidase (POP) fold in general, but the propeller of POP consists of seven blades. The propeller domain is positioned to function as a sizing filter for substrates to the active site, limiting access through either the central propeller pore of ~ 13 Å or a larger pore

of ~ 20 Å located on the side of the propeller. Globular proteins that do not fit through the pores are apparently eliminated as potential substrates, but extended peptides could reasonably access the peptidase activity through either pore.

Comparison with Other DPP-IV Structures. The structure of the rat protein is very similar to other X-ray crystal structures of DPP-IV that have recently been described and are available from public databases, which include recombinant human DPP-IV (21–25) and natural source porcine DPP-IV (26). Being roughly 83% identical in amino acid sequence to both the human and porcine isoforms, the rat structure is very similar, yielding a rms deviation of ~ 0.75 Å for positional differences of α -carbon atoms aligned with both porcine and human structures. The dimer relationship

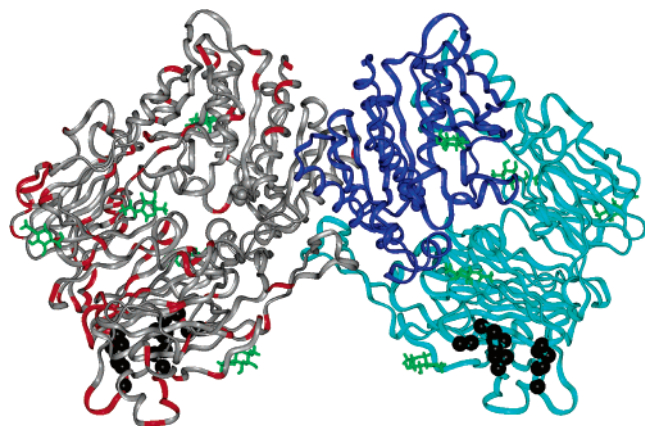


FIGURE 2: Molecular dimerization and sequence conservation. The dimer of rat DPP-IV molecules is depicted with one monomer colored by amino acid sequence conservation with human DPP-IV, where identical residues are colored gray and nonconserved residues red. The second monomer is colored by domain, with the N-terminal propeller domain colored light blue and the C-terminal catalytic domain colored dark blue. Glycosylation sites are highlighted with licorice representations of *N*-acetylglucosamine units colored green. The location of the corresponding interface with ADA for the human homologue is highlighted with black spheres.

is preserved in all structures (Figure 2), but the tetrameric arrangement of the porcine crystal structure is unique and is not observed here in the rat structure or in any structures of human DPP-IV. In contrast to the porcine and human DPP-IV structures, which were determined at high pH (pH ≥ 8), the rat structure was determined at low pH (pH 5). While a study of the pH profile indicated an optimal pH of 8 for human DPP-IV activity with little or no activity at acidic pH (27), the close agreement of the structures shows that the general tertiary structure is not influenced by pH. Residues in the active site are especially well conserved among the species, as are the atomic positions upon structural alignment. In the vicinity of the active site, the rat structure differs at Gly207, which is a serine in the human form and located 14 Å from the catalytic serine, Ser631. Other differences among the structures are observed progressively farther from the active site to the exterior surface of the protein, with amino acid differences more prevalent in the propeller domain than the catalytic domain.

In addition to amino acid changes that cause local structural differences among homologues, other differences arise from varied glycosylation patterns of the proteins. Electron density is observed for carbohydrate attached to the protein, giving a direct image of five asparagine-linked attachment sites for the rat protein and modeled as *N*-acetylglucosamine units on residues Asn83, Asn90, Asn227, Asn319, and Asn521. The first four sites are located on the external surface of the propeller, and the fifth site resides on the exterior of the catalytic domain. Glycosylation is also observed in other DPP-IV structures with subtle variations for each, and although the patterns vary, glycosylation of individual sites is not necessary for enzymatic activity, dimer formation, or ADA binding, as investigated in studies of the human enzyme (28).

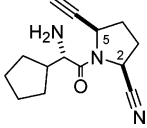
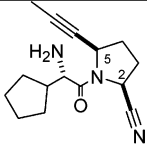
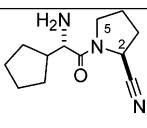
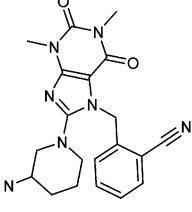
In contrast to many species, rat DPP-IV does not bind adenosine deaminase (ADA), a ubiquitous enzyme found in all mammals. While the functional consequences of ADA binding are not yet fully understood, we can assess the

structural features that yield species differences. A cryo-EM study of human DPP-IV bound to ADA revealed the interacting surface centers on DPP-IV residues Leu294 and Val341 (6). The location of the interaction is consistent with data that show point mutants of human DPP-IV residues Leu340, Val341, Ala342, and Arg343 each lack the ability to bind ADA (29). The interaction was further illuminated by a crystal structure of a complex between human DPP-IV and bovine ADA, revealing the detailed complementary interactions of an amphipathic interface (7). Residues of ADA directly involved in complex formation with DPP-IV are largely conserved between the human and rat forms, and affinity differences between the species are thought to be primarily due to variation in DPP-IV. Rat DPP-IV does not differ dramatically in structure from the porcine or human species over the region corresponding to the ADA interface, but replacements of hydrophilic for hydrophobic residues subtly alter the nature of the protein surface. In particular, Leu294 and Ile295 in human DPP-IV are replaced by Thr292 and Thr293 in rat DPP-IV, respectively, and while they occupy the same location upon superposition of the protein structures, the hydrophilic residues of rat are not complementary for ADA binding. Also, in the structure of the complex, Arg336 in human DPP-IV forms a salt bridge interaction with ADA, but the corresponding residue in rat DPP-IV is Val334, which again is located in the same position upon structural alignment but is clearly incapable of mimicking the same interaction with ADA. Taken together, the differences reasonably account for the reduced affinity of both rat and human ADA for rat DPP-IV.

Selective DPP-IV Inhibition with Alkynyl Cyanopyrrolidines. The focus of our efforts was to obtain structural information relevant to designing an optimal small molecule inhibitor of DPP-IV. Prior to determining the structure of rat DPP-IV, we created a homology model of the enzyme by methods analogous to those reported by other workers (30) and examined models of acylated cyanopyrrolidine inhibitors (11). While much of the active site was approximate in this modeling, the availability of unoccupied volume near the 5 position, but not the 3 or 4 position of a docked pyrrolidine inhibitor, suggested prioritization of 5-substituted analogues for evaluation. In the ensuing exploratory chemistry effort, a marked preference for small alkynyl substituents at this position was discovered. Compounds **1** and **2** are specific examples of compounds from these series and have relatively potent inhibitory activity for DPP-IV (Table 2). The design of these compounds includes substratelike features containing a carbonyl and basic amine as would be found in the peptide backbone at the N-terminus of a substrate, and a "side chain" for the amino acid at the P2 position consisting of a cyclopentyl moiety.

Interestingly, the alkynyl substituent at the 5 position confers significant enzyme selectivity. In particular, compounds **1** and **2** have inhibitory K_i values of >10000 nM for DPP-8 and DPP-9, whereas the corresponding analogue with H in the 5 position, compound **3**, has a low-nanomolar potency for DPP-IV, DPP-8, and DPP-9 (Table 2). Incidentally, such potency discrimination among peptidase family members is likely important in clinical therapy, because a recent study suggests inhibition of DPP-8 and/or DPP-9 results in toxicity to animals (31). To understand the binding of these selective compounds to DPP-IV, we examined the

Table 2: Compounds and Peptidase Inhibition

| | Compound | Rat DPP-IV Ki (nM) | Human DPP-IV Ki (nM) | Human DPP8 Ki (nM) |
|---|--|--------------------------|----------------------------|--------------------------|
| 1 |  | 12 | 8 | 17,700 |
| 2 |  | 56 | 30 | >30,000 |
| 3 |  | 1 | 1 | 4 |
| 4 |  | 3 | 2 | >30,000 |

structure and noted the restricted space surrounding the S1 pocket, which suggested the necessity of protein movement to accommodate the compounds, yet structure determination of inhibitor complexes was necessary to detail these differences.

Structures Exhibit Flexible Accommodation of Alkynyl Cyanopyrrolidines. A simple soaking protocol coupled with the inherent high level of symmetry of the cubic crystals facilitated experimental structure determination of rat DPP-IV in complex with inhibitors. X-ray data were collected on crystals separately soaked in compounds **1** and **2**, and electron density maps clearly reveal the presence of compound in the active site (Figure 3). Continuous density extending from the active site serine residue, Ser631, demonstrates the covalent nature of inhibition for these compounds, and structures were built and refined to the experimental data. Consistent with earlier structural reports of cyanopyrrolidine inhibitors (23, 26), the pyrrolidine ring nestles into a hydrophobic pocket in the S1 position of the active site (Figure 4). For these compounds, the nitrile forms an imidate adduct with the hydroxyl of Ser631, the carbonyl oxygen is positioned to form a hydrogen bond with the side chain of Asn711, and the primary amine sits between a pair

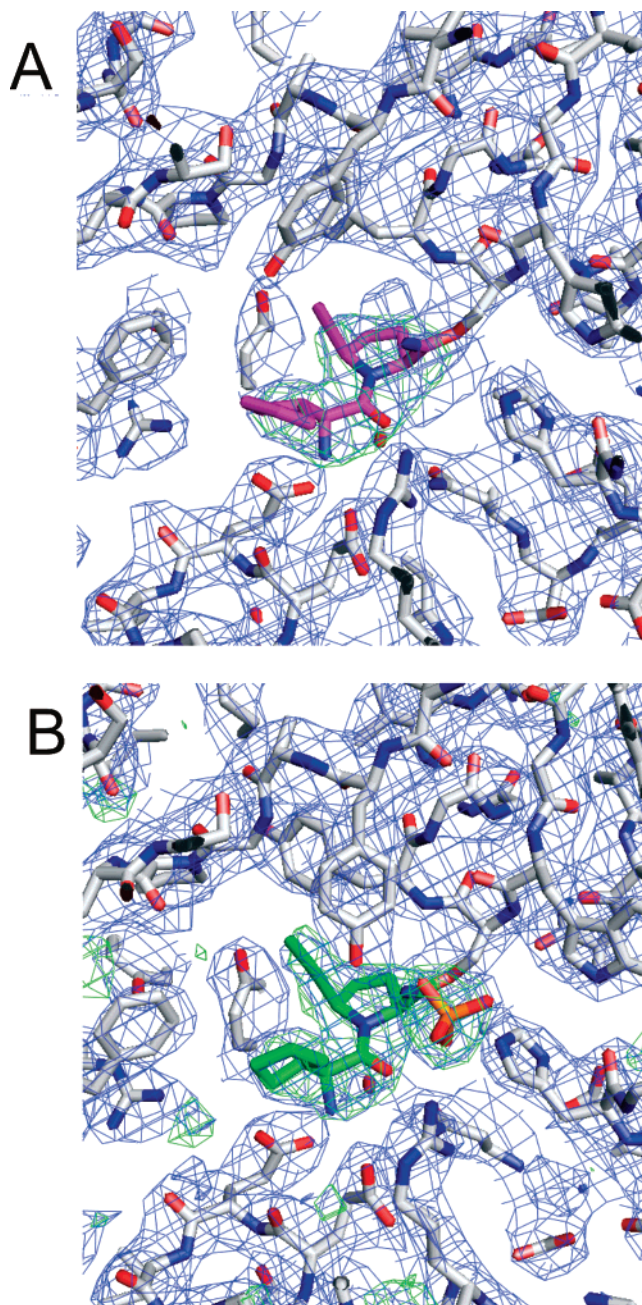


FIGURE 3: X-ray structures of rat DPP-IV with alkynyl cyanopyrrolidines. The covalent complexes of rat DPP-IV (gray) with (A) compound **1** (magenta) and (B) compound **2** (green) are shown. Difference Fourier $2F_o - F_c$ electron density maps (blue) and $F_o - F_c$ compound omit maps (green) are contoured at 1σ and 3σ , respectively.

of glutamate residues, Glu203 and Glu204, forming an electrostatic interaction with the acidic side chains. Importantly, these interactions mimic recognition determinants noted for DPP-IV substrates in the P1 and P2 positions, where the primary amine, the carbonyl oxygen, and the pyrrolidine ring correspond to elements of the first and second residues of a peptide substrate. The cyclopentyl moiety interacts with Phe355, extending in the direction that the side chain of the first residue (P2 position) of a substrate would be expected to occupy. Given the broad solvent exposure of this region, any amino acid side chain could conceivably fit into the cavity in such an arrangement with the substrate's N-terminus pinned by an interaction with

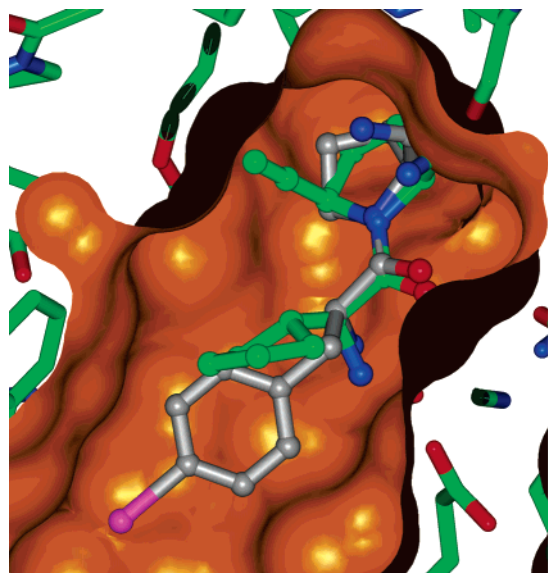


FIGURE 4: Structural comparison of cyanopyrrolidine inhibitors. The inhibitor complex of rat DPP-IV with compound **2** (green) is shown with a superimposed overlay of the porcine DPP-IV complex (PDB entry 1ORW) with a cyanopyrrolidine inhibitor lacking substitution at the 5 position (gray).

Glu203/Glu204, and the lack of specificity for residues in the P2 position of DPP-IV substrates is readily rationalized.

The alkynyl moiety of both compounds **1** and **2** is accommodated in a restricted location that is bounded by the side chain of Tyr548 at the front edge of the S1 pocket. In the complex with compound **1**, the OH group of Tyr548 is oriented toward the terminal ethynyl carbon of the inhibitor at a distance of 3.3 Å, suggesting a favorable van der Waals interaction. For compound **2**, the additional bulk of the terminal methyl cannot be accommodated in exactly the same way, and the relative position of Tyr548 is shifted to the “right” (Figure 5), accommodating the increased volume of the larger propynyl substituent. In this case, the OH group

of Tyr548 is within 2.9 Å of the imidate formed by the covalent adduct, suggesting a different H-bonding pattern for the enzyme–inhibitor complex. In fact, with this environment an adventitious binding site for a sulfate anion from the crystallization buffer is formed among Tyr548, the imidate adduct, and the side chain of Arg123 as judged by the electron density map (Figure 3). When the structures are overlaid, the difference in the position of the OH group of Tyr548 for the two complexes is 3.3 Å, which actually only partially captures the conformational difference of Tyr548 between the structures, because the plane of the side chain is also rotated (15° for χ_1 and 40° for χ_2), altering the solvent-exposed surface of the protein. Tyr548 in the apo structure is located in an intermediate conformation relative to the structures of the two complexes observed here, indicating that a range of positions is possible.

The Xanthine Analogue Requires a Similar Conformational Change of Tyr548 for DPP-IV Inhibition. In other exploratory studies, screening of the Abbott compound collection revealed several xanthine-based analogues as inhibitors of DPP-IV, but we soon discovered our medicinal chemistry efforts paralleled those of others (18). Compound **4** was readily prepared as a potent inhibitor with a K_i value of 2 nM for DPP-IV in our assay but interestingly does not inhibit DPP-8 to any measurable extent. To examine the mode of inhibition, X-ray data were collected on a crystal of rat DPP-IV complexed with compound **4** that diffracted to 3.3 Å resolution. The resulting difference Fourier electron density maps reveal the compound bound in the active site (Figure 6), and conformational flexibility of Tyr548 is immediately found to be critically important. In this case, the side chain of Tyr548 adopts a position very similar to that observed in the complex with compound **1**; however, the detailed interactions are quite different. The aromatic 5,6-bicyclic xanthine core is located beside the side chain of Tyr548, oriented for a π – π stacking interaction, while the phenyl moiety fits into the S1 pocket of the protein. In this pose,

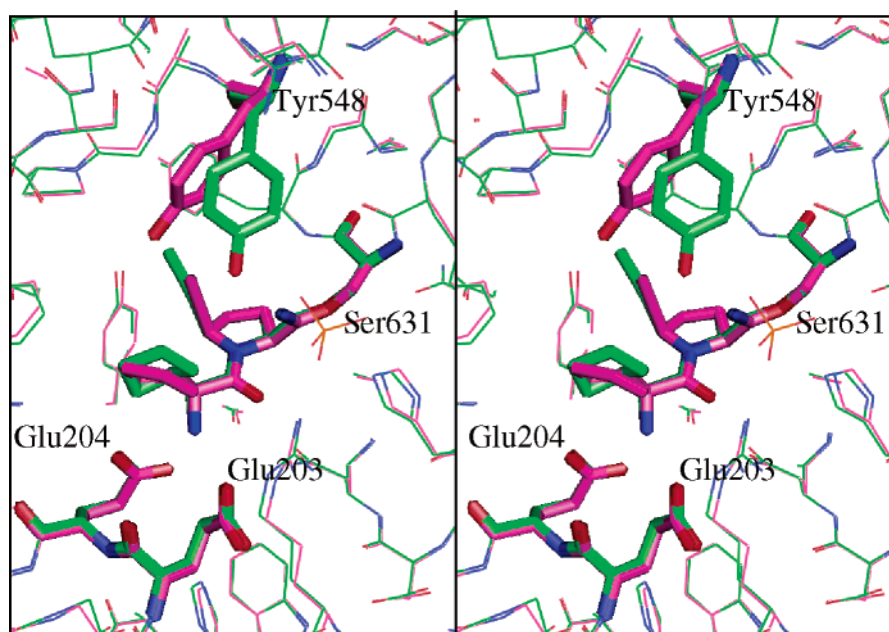


FIGURE 5: Superposition of rat DPP-IV inhibitor complexes with alkynyl cyanopyrrolidines (stereoview). The structures of rat DPP-IV with compound **1** (magenta) and compound **2** (green) are aligned, highlighting the difference in positions for Tyr548 (thick bonds). Both compounds form a covalent bond with the active site serine residue, Ser631 (thick bonds).

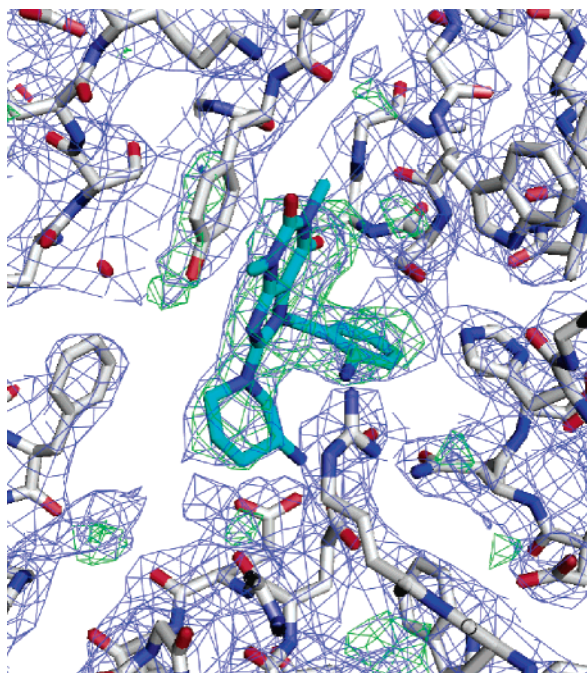


FIGURE 6: X-ray structure of rat DPP-IV with a noncovalent xanthine analogue. Inhibitor **4** is highlighted in blue. The electron density is contoured at 1σ for the $2F_o - F_c$ (blue) map and at 3σ for the initial $F_o - F_c$ (green) difference map calculated without the compound.

the compound is positioned to form a H-bond (2.8 \AA) between its carbonyl oxygen and the backbone amide of Tyr632. The cyano substituent on the phenyl ring does not react like the cyanopyrrolidines to form a covalent adduct with the active site Ser631, but rather it is oriented for a favorable polar interaction with the side chain of Arg123 at a distance of 3.1 \AA . Density for the saturated ring with the basic amine extends toward Glu203/Glu204, but the data do not allow the details of its ring pucker conformation to be meaningfully resolved. During the preparation of this paper,

the structure of a similar compound bound to porcine DPP-IV was reported, and the binding mode is consistent with the results presented here (32).

Because xanthine compound **4** does not bind covalently, we decided to use it as a tool to test the reversibility of the covalent inhibition of the cyanopyrrolidines. A crystal was soaked in the presence of cyanopyrrolidine compound **1** for 24 h under conditions previously established to fully saturate the active site with inhibitor, and after soaking in buffer without inhibitor for a washout period of 72 h, the crystal was soaked in the presence of compound **4** for 24 h and preserved. X-ray data were collected on the crystal, and the resulting electron density map clearly revealed the presence of compound **4** without any evidence of the cyanopyrrolidine. This suggests that although cyanopyrrolidine compound **1** binds covalently, the compound can be displaced. We recently also learned of a report detailing enzyme kinetics studies of DPP-IV with a cyanopyrrolidine inhibitor that shows evidence of reversibility of covalent adduct formation, and the proposed mechanism is consistent with our observations of apparent reversibility (33).

Induced Conformational Changes of Tyr548 Promote DPP-IV Selectivity. Xanthine analogue compound **4** induces a subtle conformational change for Tyr548 that was not readily anticipated, and the observed binding mode was unexpected. In the apo structure, the side chain of Tyr548 occludes the backbone amide of Tyr632, and its H-bond with the compound was not easily predicted. Interestingly, compound **1** and compound **4** stabilize the protein in similar conformations even though they are of very different chemotypes (Figure 7). In different ways, both compounds fill the hydrophobic S1 pocket, and both compounds interact with the Glu203/Glu204 acidic pair via a basic amine. While the conformation of Tyr548 appears marginally favorable with compound **1**, the same protein conformation seems crucial for complex formation with compound **4**, and therein

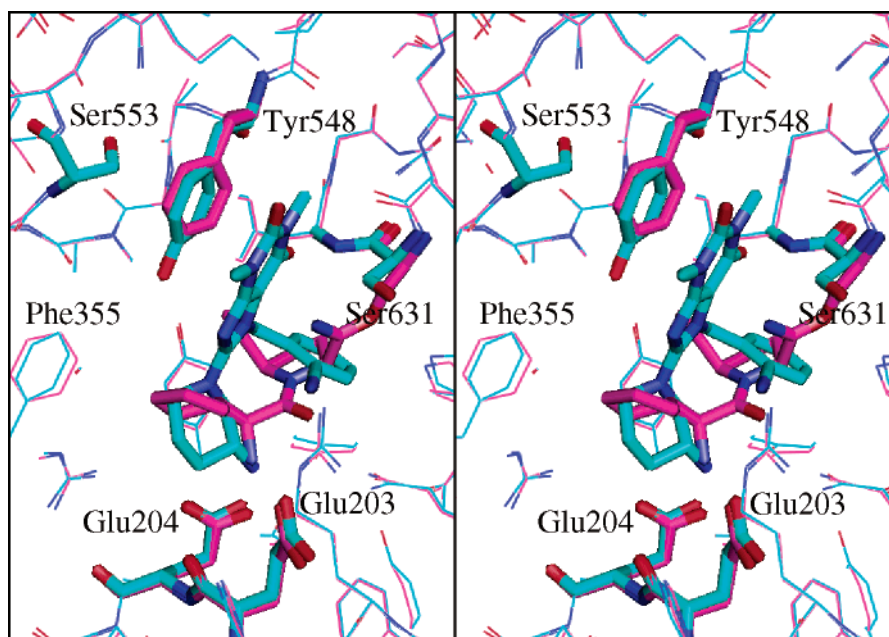


FIGURE 7: Structural comparison of rat DPP-IV complexes with peptidase-selective inhibitors (stereoview). The structures with compound **1** (magenta) and compound **4** (blue) are aligned, and residues noted in the text are highlighted. The location of Ser553 is shown, and its proximity to Tyr548 is proposed to be the basis of inhibitor selectivity for DPP-IV over DPP-8 and DPP-9, which both contain a bulkier valine residue in the position corresponding to Ser553.

suggestive of a structural basis for the observed peptidase selectivity.

The conformational modulation of Tyr548 observed in the inhibitor complexes is likely important for the selectivity these compounds exhibit for DPP-IV over DPP-8 and DPP-9. Notably, Tyr548 is of critical functional importance, and the corresponding residue in the human DPP-IV enzyme is conserved as Tyr547, which directly participates in the formation of the tetrahedral intermediate of the substrate with Ser631 during catalysis (24, 25, 34). Although the three-dimensional structures of DPP-8 and DPP-9 are not available for comparison, the corresponding tyrosine residue is conserved in sequence alignments, but modeling suggests it does not have the same conformational mobility in DPP-8 or DPP-9 as in DPP-IV due to a replacement of the neighboring Ser553 with a bulkier valine residue. In the DPP-IV structures with compounds **1** and **4**, Tyr548 is shifted from its apo position to within van der Waals contact of Ser553 (Figure 7), which in both DPP-8 and DPP-9 is a valine residue that would be predicted to interfere with a corresponding shift due to its increased steric bulk. In the case of compound **2**, Tyr548 is shifted in an opposite direction that is not expected to be restricted in DPP-8 or DPP-9, yet the relatively poor inhibitory activity toward DPP-8 suggests the propynyl substituent probes a region of difference between the peptidases.

The energetic cost for rearrangement of Tyr548 is apparently fairly small, because the compounds are quite potent inhibitors of DPP-IV. In this case, the 4-fold difference in potency between compounds **1** and **2** is not dramatic and does not especially suggest a difference in the shape of the active site, yet the three-dimensional structure–activity relationship reveals an important structural property change that might be exploited further in inhibitor design. The observed adaptability of the active site architecture suggests potent inhibitors might be designed with alternative binding modes, optimizing interactions not apparent from the apo-protein conformation.

In conclusion, we report the crystal structure of DPP-IV isolated from rat and draw comparisons with previously reported structures of DPP-IV from human and porcine species. While there are many similarities, subtle differences are evident in the residue variation, particularly in the ADA-binding region, and the natural glycosylation pattern. Experimental structure determination of DPP-IV in complex with inhibitory compounds offers insight into features such as protein flexibility that are valuable for structure-based drug design. We illustrate the accommodation of substituents at the 5 position of the pyrrolidine–nitrile inhibitors as an important avenue of analogue variation. In two inhibitor-bound structures, the 5-alkyne group is located close to the side chain of Tyr548, and specific differences cause different conformations of the tyrosine side chain. Similar conformational adaptability of Tyr548 is demonstrated in the structure of the complex with a potent xanthine analogue inhibitor. We suggest that, although Tyr548 is conserved, its conformational flexibility is different for DPP-IV versus that for other peptidase family members, and synthetic compounds can utilize this difference for selective DPP-IV inhibition.

ACKNOWLEDGMENT

Data were collected at beamline 17-ID in the facilities of the Industrial Macromolecular Crystallography Association Collaborative Access Team (IMCA-CAT) at the Advanced Photon Source. These facilities are supported by the companies of the Industrial Macromolecular Crystallography Association.

REFERENCES

- Wiedeman, P. E., and Trevillyan, J. M. (2003) Dipeptidyl peptidase IV inhibitors for the treatment of impaired glucose tolerance and type 2 diabetes, *Curr. Opin. Invest. Drugs* 4, 412–20.
- Holst, J. J. (2004) Treatment of type 2 diabetes mellitus with agonists of the GLP-1 receptor or DPP-IV inhibitors, *Expert Opin. Emerging Drugs* 9, 155–66.
- Drucker, D. J. (2002) Biological actions and therapeutic potential of the glucagon-like peptides, *Gastroenterology* 122, 531–44.
- Deacon, C. F. (2004) Therapeutic strategies based on glucagon-like peptide 1, *Diabetes* 53, 2181–9.
- Aytac, U., and Dang, N. H. (2004) CD26/dipeptidyl peptidase IV: A regulator of immune function and a potential molecular target for therapy, *Curr. Drug Targets: Immune, Endocr. Metab. Disord.* 4, 11–8.
- Ludwig, K., Fan, H., Dobers, J., Berger, M., Reutter, W., and Bottcher, C. (2004) 3D structure of the CD26-ADA complex obtained by cryo-EM and single particle analysis, *Biochem. Biophys. Res. Commun.* 313, 223–9.
- Weihofen, W. A., Liu, J., Reutter, W., Saenger, W., and Fan, H. (2004) Crystal structure of CD26/DPP-IV in complex with adenosine deaminase reveals a highly amphiphilic interface, *J. Biol. Chem.* 279, 43330–5.
- Lambeir, A. M., Durinx, C., Scharpe, S., and De Meester, I. (2003) Dipeptidyl-peptidase IV from bench to bedside: An update on structural properties, functions, and clinical aspects of the enzyme DPP IV, *Crit. Rev. Clin. Lab. Sci.* 40, 209–94.
- Rosenblum, J. S., and Kozarich, J. W. (2003) Prolyl peptidases: A serine protease subfamily with high potential for drug discovery, *Curr. Opin. Chem. Biol.* 7, 496–504.
- Schechter, I., and Berger, A. (1967) On the size of the active site in proteases. I. Papain, *Biochem. Biophys. Res. Commun.* 27, 157–62.
- Li, J., Wilk, E., and Wilk, S. (1995) Aminoacylpyrrolidine-2-nitriles: Potent and stable inhibitors of dipeptidyl-peptidase IV (CD 26), *Arch. Biochem. Biophys.* 323, 148–54.
- Ahren, B., Landin-Olsson, M., Jansson, P. A., Svensson, M., Holmes, D., and Schweizer, A. (2004) Inhibition of dipeptidyl peptidase-4 reduces glycemia, sustains insulin levels, and reduces glucagon levels in type 2 diabetes, *J. Clin. Endocrinol. Metab.* 89, 2078–84.
- Otwinowski, Z., and Minor, W. (1997) Processing of X-ray Diffraction Data Collected in Oscillation Mode, *Methods Enzymol.* 276, 307–26.
- French, S., and Wilson, K. (1978) On the Treatment of Negative Intensity Observations, *Acta Crystallogr.* A34, 517–25.
- Collaborative Computational Project Number 4 (1994) The CCP4 Suite: Programs for Protein Crystallography, *Acta Crystallogr.* D50, 760–3.
- Terwilliger, T. C., and Berendzen, J. (1999) Automated MAD and MIR structure solution, *Acta Crystallogr.* D55, 849–61.
- Jones, T. A., Zou, J. Y., Cowan, S. W., and Kjeldgaard, M. (1991) Improved methods for building protein models in electron density maps and the location of errors in these models, *Acta Crystallogr.* A47, 110–9.
- Himmelsbach, F., Mark, M., Eckhardt, M., Langkopf, E., Maier, R., and Lotz, R. (2002) World Patent Appl. WO2002068420.
- Madar, D., Pei, Z., Pireh, D., Djuric, S. W., Wiedeman, P. E., Yong, H., Feenstra, M. J., Kopecka, H., Li, X., Longenecker, K. L., Sham, H., Stewart, K. D., and Szczepankiewicz, B. G. (2004) World Patent Appl. WO2004026822.
- Fulop, V., Bocskei, Z., and Polgar, L. (1998) Prolyl oligopeptidase: An unusual β -propeller domain regulates proteolysis, *Cell* 94, 161–70.
- Rasmussen, H. B., Branner, S., Wiberg, F. C., and Wagtmann, N. (2003) Crystal structure of human dipeptidyl peptidase IV/CD26 in complex with a substrate analog, *Nat. Struct. Biol.* 10, 19–25.

22. Hiramatsu, H., Kyono, K., Higashiyama, Y., Fukushima, C., Shima, H., Sugiyama, S., Inaka, K., Yamamoto, A., and Shimizu, R. (2003) The structure and function of human dipeptidyl peptidase IV, possessing a unique eight-bladed β -propeller fold, *Biochem. Biophys. Res. Commun.* 302, 849–54.
23. Oefner, C., D'Arcy, A., MacSweeney, A., Pierau, S., Gardiner, R., and Dale, G. E. (2003) High-resolution structure of human apo dipeptidyl peptidase IV/CD26 and its complex with 1-[(2-[(5-iodopyridin-2-yl)amino]-ethyl)amino]-acetyl]-2-cyano-(S)-pyrrolidine, *Acta Crystallogr. D* 59, 1206–12.
24. Thoma, R., Löffler, B., Stihle, M., Huber, W., Ruf, A., and Hennig, M. (2003) Structural basis of proline-specific exopeptidase activity as observed in human dipeptidyl peptidase-IV, *Structure* 11, 947–59.
25. Aertgeerts, K., Ye, S., Tennant, M. G., Kraus, M. L., Rogers, J., Sang, B. C., Skene, R. J., Webb, D. R., and Prasad, G. S. (2004) Crystal structure of human dipeptidyl peptidase IV in complex with a decapeptide reveals details on substrate specificity and tetrahedral intermediate formation, *Protein Sci.* 13, 412–21.
26. Engel, M., Hoffmann, T., Wagner, L., Wermann, M., Heiser, U., Kiefersauer, R., Huber, R., Bode, W., Demuth, H. U., and Brandstetter, H. (2003) The crystal structure of dipeptidyl peptidase IV (CD26) reveals its functional regulation and enzymatic mechanism, *Proc. Natl. Acad. Sci. U.S.A.* 100, 5063–8.
27. Leiting, B., Pryor, K. D., Wu, J. K., Marsilio, F., Patel, R. A., Craik, C. S., Ellman, J. A., Cummings, R. T., and Thornberry, N. A. (2003) Catalytic properties and inhibition of proline-specific dipeptidyl peptidases II, IV and VII, *Biochem. J.* 371, 525–32.
28. Aertgeerts, K., Ye, S., Shi, L., Prasad, S. G., Witmer, D., Chi, E., Sang, B. C., Wijnands, R. A., Webb, D. R., and Swanson, R. V. (2004) N-linked glycosylation of dipeptidyl peptidase IV (CD26): Effects on enzyme activity, homodimer formation, and adenosine deaminase binding, *Protein Sci.* 13, 145–54.
29. Abbott, C. A., McCaughan, G. W., Levy, M. T., Church, W. B., and Gorrell, M. D. (1999) Binding to human dipeptidyl peptidase IV by adenosine deaminase and antibodies that inhibit ligand binding involves overlapping, discontinuous sites on a predicted β propeller domain, *Eur. J. Biochem.* 266, 798–810.
30. Reva, B., Finkelstein, A., and Topiol, S. (2002) Threading with chemostructural restrictions method for predicting fold and functionally significant residues: Application to dipeptidyl peptidase IV (DPP-IV), *Proteins* 47, 180–93.
31. Lankas, G. R., Leiting, B., Roy, R. S., Eiermann, G. J., Beconi, M. G., Biftu, T., Chan, C. C., Edmondson, S., Feeney, W. P., He, H., Ippolito, D. E., Kim, D., Lyons, K. A., Ok, H. O., Patel, R. A., Petrov, A. N., Pryor, K. A., Qian, X., Reigle, L., Woods, A., Wu, J. K., Zaller, D., Zhang, X., Zhu, L., Weber, A. E., and Thornberry, N. A. (2005) Dipeptidyl peptidase IV inhibition for the treatment of type 2 diabetes: Potential importance of selectivity over dipeptidyl peptidases 8 and 9, *Diabetes* 54, 2988–94.
32. Engel, M., Hoffmann, T., Manhart, S., Heiser, U., Chambre, S., Huber, R., Demuth, H. U., and Bode, W. (2006) Rigidity and flexibility of dipeptidyl peptidase IV: Crystal structures of and docking experiments with DPIP, *J. Mol. Biol.* 355, 768–83.
33. Kim, Y. B., Kopcho, L. M., Kirby, M. S., Hamann, L. G., Weigelt, C. A., Metzler, W. J., and Marcinkiewicz, J. (2006) Mechanism of Gly-Pro-pNA cleavage catalyzed by dipeptidyl peptidase-IV and its inhibition by saxagliptin (BMS-477118), *Arch. Biochem. Biophys.* 445, 9–18.
34. Bjelke, J. R., Christensen, J., Branner, S., Wagtmann, N., Olsen, C., Kanstrup, A. B., and Rasmussen, H. B. (2004) Tyrosine 547 constitutes an essential part of the catalytic mechanism of dipeptidyl peptidase IV, *J. Biol. Chem.* 279, 34691–7.

BI060184F